Available online at www.sciencedirect.com

SciVerse ScienceDirect

Ceramics International 38 (2012) 2865–2872

CERAMICS INTERNATIONAL

www.elsevier.com/locate/ceramint

Electrical characterization of room temperature humidity sensors in $La_{0.8}Sr_{0.2}Fe_{1-x}Cu_xO_3$ ($x = 0$, 0.05, 0.10)

A. Cavalieri [a], T. Caronna [b], I. Natali Sora [b], J.M. Tulliani [a,*]

[a] *Materials Science and Chemical Engineering Department, Politecnico di Torino, corso Duca degli Abruzzi 24, 10129 Torino, Italy*
[b] *INSTM R.U. and Industrial Engineering Department, Università di Bergamo, viale Marconi 5, 24044 Dalmine, Italy*

Received 24 August 2011; received in revised form 21 November 2011; accepted 22 November 2011
Available online 20 January 2012

Abstract

Semiconducting oxide gas sensors based on $La_{0.8}Sr_{0.2}Fe_{1-x}Cu_xO_3$ ($x = 0$, 0.05, 0.10) (LSF, LSFC05, and LSFC10, respectively) were prepared by screen-printing for humidity detection at room temperature.

The thick-films were heat-treated at 800, 900 and 1000 °C for 1 h and all the compositions proved to be effective in humidity sensing and presented a good reproducibility between several measurements. However, the best results were obtained with LSFC10 fired at 800 °C which showed a detection limit of 15% relative humidity and a maximum sensor response of about 87%, higher than the previous results. Copper addition to lanthanum strontium ferrites proved to be effective in lowering the sensors' detection limit.

Keywords: A. Films; C. Electrical properties; D. Ferrites; E. Sensors; Copper doping

1. Introduction

Lanthanum ferrites have been widely studied for use in catalysis [1–4], as cathode materials for solid oxide fuel cells (SOFCs) [5–11] and in chemical sensor applications [12–15], e.g. in the chemical and food industries, and for environmental monitoring. As many semiconductor-based chemical sensors, they owe their attractiveness to their small size, simple operation and high sensitivity.

In perovskite-type oxides (ABO_3), the atoms on site "A" are susceptible to humidity. Humidity sensitivity characteristics can be enhanced by partially substituting A site atoms with rare earth elements [16]. The stability of perovskite oxides allows the partial substitution of other ions at both "A" and "B" sites without changing the basic perovskite structure. However, this substitution can lead to oxygen vacancies, variable "B" site cation valences and crystalline structure defects, which then directly or indirectly affect oxygen permeation and catalytic activity [17]. For example, many studies have focused on the effect of alkaline earth (Mg^{2+}, Ca^{2+}, Sr^{2+}) doping on the conductivity, sintering and stability of $ACrO_3$ perovskite systems, but less attention has been paid to the possible application of these materials as sensors [18].

Recently, $LaCo_xFe_{11-x}O_{3-\delta}$ humidity sensing properties have been extensively studied, as well as the effect of K-substitution at the La-site [17] on the sensor response.

In the literature, $La_{1-x}Sr_xFeO_3$ ($0.1 \leq x \leq 0.4$, LSF) has already been proposed as a room temperature humidity sensing material. It has been observed that its resistance increases with increasing relative humidity, while its sensitivity increases with an increase in the x value [19].

The partial substitution of Fe^{3+} with Cu^{2+} in $La_{0.8}Sr_{0.2}FeO_3$ results in the compound formula of $La_{0.8}Sr_{0.2}Fe_{1-x}Cu_xO_3$ ($x = 0$, 0.05, 0.10) (LSF, LSFC05 and LSFC10, respectively).

As Cu-doped lanthanum strontium ferrites can be used as intermediate temperature (IT)-SOFCs cathode materials, the electrical conductivity behavior has been previously studied with respect to P_{O_2} and temperature [20]. However, little is known about the effect of Cu doping on their humidity sensing properties and mechanisms.

In this work, thick-films of Cu-doped lanthanum strontium ferrites, LSFC05 and LSFC10 are proposed as alternatives to

* Corresponding author. Tel.: +39 011 090 47 00; fax: +39 011 090 46 99.
E-mail address: jeanmarc.tulliani@polito.it (J.M. Tulliani).

0272-8842/$36.00
doi:10.1016/j.ceramint.2011.11.059

lanthanum strontium ferrites (LSF). The screen-printing technique has been chosen because it is a simple, fast and cheap method to prepare sensors for humidity detection.

In particular, the application of $La_{0.8}Sr_{0.2}Fe_{1-x}Cu_xO_3$ based solid-state sensors is envisaged, for example, in industrial processes and in air-conditioning systems for the automatic regulation of living environments, where it is important to evaluate partial water pressure [21].

The prepared powders were first characterized by X-ray diffraction, scanning electron microscopy and nitrogen adsorption/desorption isotherm at 77 K. Then, the dependence of electrical response of the thick-films on the relative humidity (RH) was investigated. The results show that they can be proposed as materials for humidity sensing devices.

2. Materials and methods

Lanthanum ferrite powders were prepared by citrate auto-combustion of dry gel obtained from a solution of corresponding nitrates in a citric acid solution [22]. Analytical grade La_2O_3, $Sr(NO_3)_2$, $Fe(NO_3)_3{\cdot}9H_2O$, $Cu(NO_3)_2{\cdot}2.5H_2O$, citric acid ($C_6H_8O_7{\cdot}H_2O$), nitric acid (HNO_3), and aqueous NH_3 were used as starting materials. A specific amount of dried La_2O_3 was dissolved in a nitric acid solution to prepare $La(NO_3)_3{\cdot}6H_2O$. Stoichiometric amounts of metal nitrates were dissolved in water (0.1 mol/L) by stirring on a hotplate and then the solution was poured into the citric acid solution, with the molar ratio of metal ions to citric acid set at 1:1. Aqueous NH_3 was added slowly until the pH was 6.8 and the solution became into transparent. The solution was then dehydrated and the dry gel was heated in air to 250 °C to start the ignition. The resulting lightweight powder was annealed at 600 °C for 3 h in air.

For each composition, phase purity, lattice symmetry, and unit-cell parameters were determined by powder X-ray diffraction. The patterns were collected at room temperature (Bruker D8 Advance diffractometer), in the 20–60° 2θ range, using Cu-$K_{\alpha 1}$ radiation (40 kV, 40 mA, $\lambda = 0.15406$ nm); the step scan was 0.02° 2θ and a scan rate of 1° 2θ min^{-1} was used. The powder XRD data were analyzed with the Rietveld technique, using the GSAS software package for full-pattern refinements [23]. The crystallite domain size was calculated using the Scherrer equation.

Specific surface areas (S.S.A.) of the above prepared powders and the 600 °C fired powders were determined using the Brunauer, Emmett, Teller (B.E.T.) method on a Micrometrics ASAP 2010 System instrument. Prior to N_2 adsorption, the samples were placed in the cell under vacuum at 573 K for 12 h.

Before the realization of the sensors, three screen-printing inks were prepared, differing between them from the sensing material: a suitable amount of ethyleneglycolmonobutyalether (Emflow, Emca Remex, USA) in which polyvinyl butyral (PVB, Poly-(vinyl butyral-co-vinyl alcohol-co-vinyl acetate), Aldrich, USA), acting as the binder, was mixed with 0.5 g of lanthanum ferrite (LSF, LSFC05 or LSFC10) powders.

Interdigitated gold electrodes (ESL EUROPE 8835 (520C)) were screen-printed onto α-Al_2O_3 planar substrates (Coors Tek, USA, ADS-96 R, 96% alumina, 0.85 cm × 5 cm) by using a rubber squeegee and a 270 mesh steel screen: after drying overnight, these devices were fired at 520 °C for 18 min with a 2 °C/min heating ramp to optimize the electrical conductivity of the electrodes, according to the ink's manufacturer recommendations. The different inks were then manually screen-printed onto the electrodes and, once dried, the sensors were heat treated at 800, 900 or 1000 °C for 1 h. The formed films had thicknesses of about 30–40 μm and areas of about 1 cm^2.

The devices were electrically characterized by using a laboratory apparatus made of a thermostated chamber working at 25 °C in which RH could be varied from 0 to 96% [24].

RH values were measured by means of a commercial humidity and temperature probe (Delta Ohm DO9406, Italy, accuracy: ±2.5% in the 5–90% RH range and −50 to 250 °C temperature range). In the system for RH measurements, compressed air was separated into two fluxes: one was dehydrated over a chromatography alumina bed, while the second one was directed through two water bubblers, generating, respectively, a dry and a humid flow. Two manual precision microvalves allowed to recombine the two fluxes into one by means of a mixer and to adjust the RH content while keeping constant the testing conditions: a flow rate of 0.05 L/s. The laboratory apparatus for sensors testing was calibrated such that to ensure a constant air flow during electrical measurements and RH was varied by steps, each one of 3 min.

Each tested sensor was alimented by an external alternating voltage ($V = 3.6$ V @ 1 kHz) and constituted a variable resistance of this electrical circuit. A multimeter (Keithley 2000) was used to measure the tension V_{DC} at the output of the circuit. The sensor resistance was determined by substituting them, in the circuit, by known resistances and then plotting a calibrating curve $R = f(V_{DC})$. Humidity measurements were realized every 3 min in the range 0–95% relative humidity.

The sensor response (SR), expressed in %, was defined as the relative variation of the starting resistance, compared with the resistance measured under gas exposure:

$$\mathrm{SR} = 100 \times \frac{|R_0 - R_g|}{R_0} \quad (1)$$

where R_0 and R_g are the starting (in the absence of the test gas) and the gas exposed (water) measured resistances of the sensors, respectively.

3. Results and discussion

3.1. Physico-chemical characterization of powders

The XRD patterns of the LSF, LSFC05 and LSFC10 powders after annealing at 1000 °C shown in Fig. 1 were indexed based on orthorhombic unit cells. The first set of refinements was made assuming as structural model the perovskite-like cell of $La_{0.8}Sr_{0.2}FeO_{3-w}$ and the symmetry of space group *Pnma* [25]. Table 1 compares structural parameters of LSF, LSFC05 and LSFC10 as determined by Rietveld

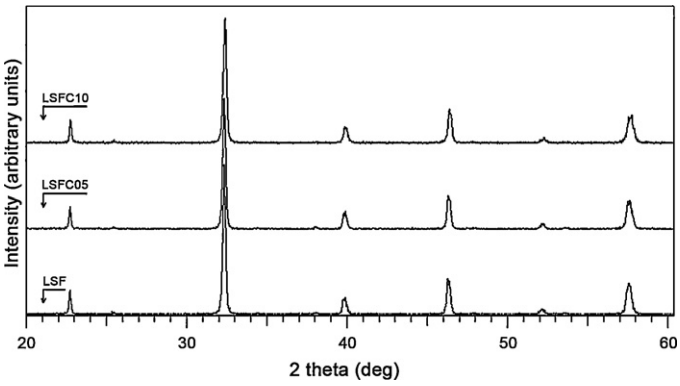

Fig. 1. X-ray powder diffraction patterns of LSF, LSFC05 and LSFC10 after annealing at 1000 °C in the 20–60° 2θ range.

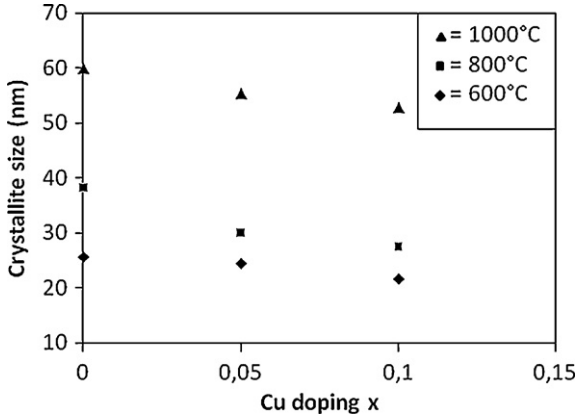

Fig. 2. Variation of crystallite size for LSF, LSFC05 and LSFC10 after annealing at 600° (black diamonds) and after further annealing at 800° (black squares) and 1000 °C (black triangles).

refinements of the XRD patterns: increasing copper content compressed the unit cell.

Crystallite sizes were calculated from powder XRD data using the Scherrer equation (Fig. 2): as the copper doping increases, the crystallite size decreases. This trend appears in samples annealed at 600 °C and in those further heat treated at 800 and 1000 °C.

The specific surface area increases with increasing amount of copper, although the values of all samples annealed at 600 °C are in the range 18–25 $m^2\ g^{-1}$.

Lanthanum ferrite powders (dispersed in ethanol and ultrasonicated for 1 min in order to break soft agglomerates) were investigated by means of a laser granulometre (Fritsch Analysette 22, Germany) prior to the preparation of the screen-printing inks: the mean diameter values of LSF, LSFC05 and LSFC10 and those corresponding to 10% and 90% of the particle size distributions are reported in Table 2. The values determined after 1 min of ultrasonication were compatible with the openings of the steel screen used during the screen-printing process.

In addition, scanning electron microscopy (SEM) observations were also carried out on green and heat treated materials (Figs. 3 and 4). It can be seen that the green powders (Fig. 3) were made of rather big grains having a high amount of pores, thus confirming the rather high specific surface area values determined by BET measurements. The 900 °C fired thick-films (Fig. 4) were characterized by a porous glassy-like microstructure and a rather large distribution of grain sizes, as already observed in the starting powders (Table 2).

3.2. Electrical characterization

Resistivity measurements in function of relative humidity are given in Figs. 5–7, in which the sensors' response is plotted against RH(%). All the sensors treated at 800 and 900 °C exhibit SRs of about 90%, while those sintered at 1000 °C show SRs smaller than 60%. This behavior is expected in samples heat treated at 800–900 °C in which the crystallite size is about half than that observed for the powders treated at 1000 °C. The results reported in Figs. 5–7 also show how the Fe substitution affects the onset of the SR. LSFC05 and LSFC10 thermal treated at 900 °C had SRs higher than 90% and started to respond for low RH values (of about 21%). Similar results were found for LSFC05 and LSFC10 heat treated at 800 °C, with the response onset at about 33 RH% (for LSFC05) and at 15 RH% (for LSFC10).

It is worth to note that the devices based on lanthanum ferrite without copper (LSF) showed higher SRs (about 80% for those sintered at 800 and 900 °C, 25% for the one treated at 1000 °C), but their onset did not change significantly (60–70 RH%).

The resistance of $LaFeO_3$ decreases with increasing relative humidity, showing the negative impedance-humidity characteristics [19]. But, the resistance of $La_{1-x}Sr_xFeO_3$ ($0.1 \leq x \leq 0.4$) increases with increasing RH, while its sensitivity increases with an increase in x value (the substituted amount of Sr). For $La_{1-x}Sr_xFeO_3$ with a positive resistance-humidity characteristic, the conduction mechanism may be as follows [19]: water molecules act as electron donors and their chemisorption decreases the electronic conductivity, depending

Table 1
Space group and refined unit cell parameters obtained from X-ray powder diffraction data.

Space group	LSF *Pnma*	LSFC05 *Pnma*	LSFC10 *Pnma*
a (Å)	5.5274(9)	5.5216(8)	5.5159(9)
b (Å)	7.821(1)	7.816(1)	7.812(1)
c (Å)	5.5538(9)	5.5520(8)	5.548(1)
V (Å^3)	240.09(7)	239.62(6)	239.04(7)

Table 2
Particle size distribution of lanthanum ferrites after 1 min of ultrasonication.

Particle size (μm)			
Sample	$Ø_{10\%}$	$Ø_{50\%}$	$Ø_{90\%}$
LSF	3.5	9.0	17.0
LSFC05	5.0	11.6	19.5
LSFC10	11.5	33.0	105.0

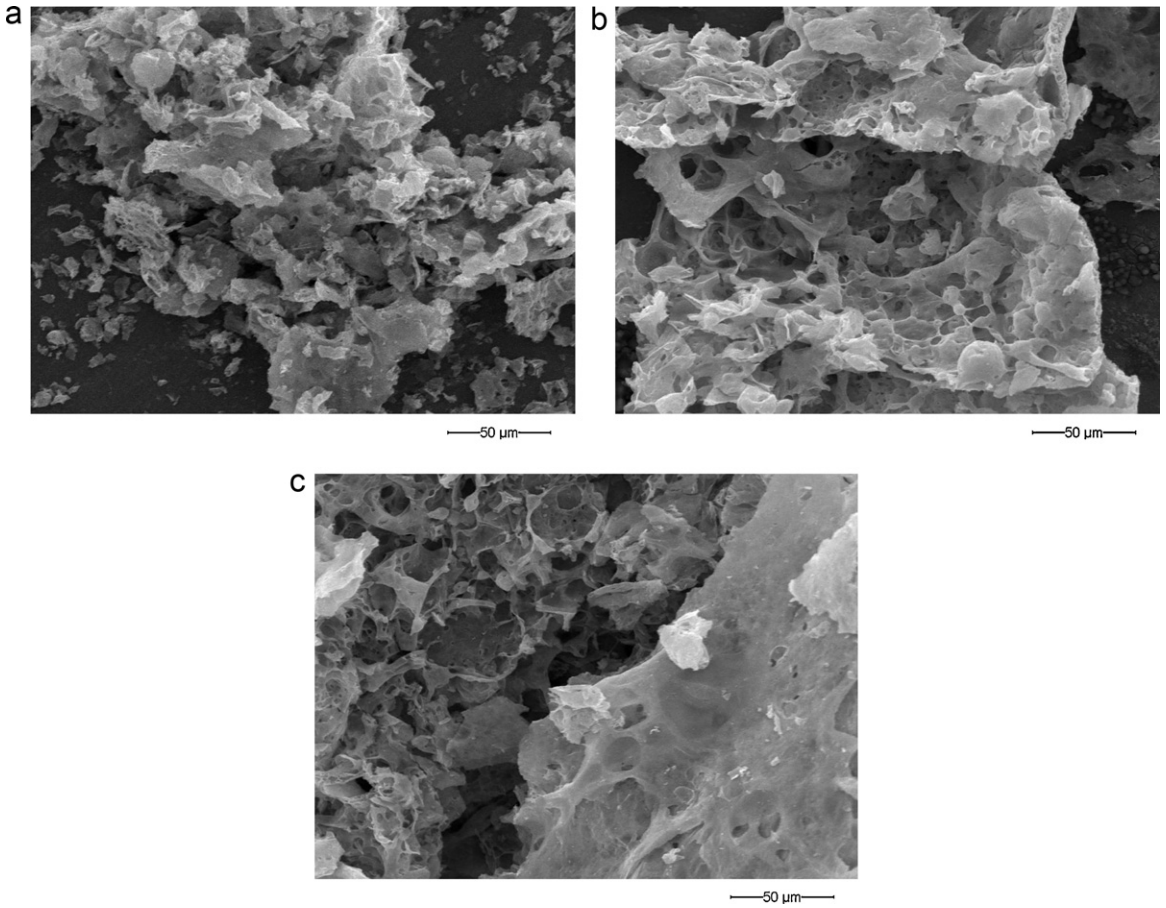

Fig. 3. SEM micrographs of green (a) LSF, (b) LSFC05 and (c) LSFC10.

on its energy band structure. N-type perovskite semiconductors exhibit electrical conductivity variation as humidity changes and have high sensitivity to water partial pressure down to 0.006 atm at elevated temperatures (400–700 °C) [26]. However, at room temperature, the porous perovskite oxides operating at room temperature may be regarded as simple resistive/capacitive ceramics [26].

From spectroscopic experiments on defective single crystals surfaces [27], it is known that chemisorption in perovskites is likely to be completed at a water pressure of the order of 0.1 Pa, and for this reason can be discarded at higher humidity levels. On the contrary, physical adsorption and capillary condensation take place in the whole range and the time required to reach equilibrium can be related to the time necessary for the H_2O pressure to establish into the various parts of the solid. As a consequence, microstructure and particularly pores size distribution must be considered to explain the electrical properties.

Since we operate at room temperature, the resistance-humidity characteristic is mainly determined by the grain surface resistance of the lanthanum ferrite-based materials. In the first stage of water adsorption, a few water vapor molecules tend to chemically adsorb on the grain surfaces of the sample giving rise to La(Sr)–OH hydroxyl groups [19]. Then, physical adsorption of water occurs through hydrogen bonding to the surface hydroxyl groups; this first adsorbed layer is localized by the hydrogen bond of a single water molecule to two surface hydroxyls, and a proton may be transferred from a La(Sr)–OH group to a water molecule to form H_3O^+ [19]. When more water vapor is adsorbed, more water molecules will cluster to form a liquid-like multilayer of hydrogen-bonded water molecules. Finally these physisorbed water molecules condense into pores with size in the mesopore range (1–250 nm).

Since the formation of clusters of H_2O and the hydration of H^+ into H_3O^+ are energetically favored in liquid water, the dominant charge carriers in the water adsorbed in the mesopores are H^+. The amount of H^+ increases when increasing the moisture content, so H^+ can move freely in liquid water, giving a decrease of grain surface resistance with increasing RH.

This mechanism explains why R_g, defined in Eq. (1), tends to decrease with increasing RH, leading to an increase of SRs, evidenced by all the sensors, though LSF is a known p-type semiconductor [19,21].

The enhanced humidity sensitivity at low RH values for Cu-doped materials, as compared with the unsubstituted samples, are probably related to the larger specific surface area.

All the sensors were characterized by a response time (the time taken to achieve 90% of the total resistance change in the case of gas adsorption) of about 300 s. The response time was calculated from the corresponding water concentration in which the sensor started to exhibit an increase in SR: these

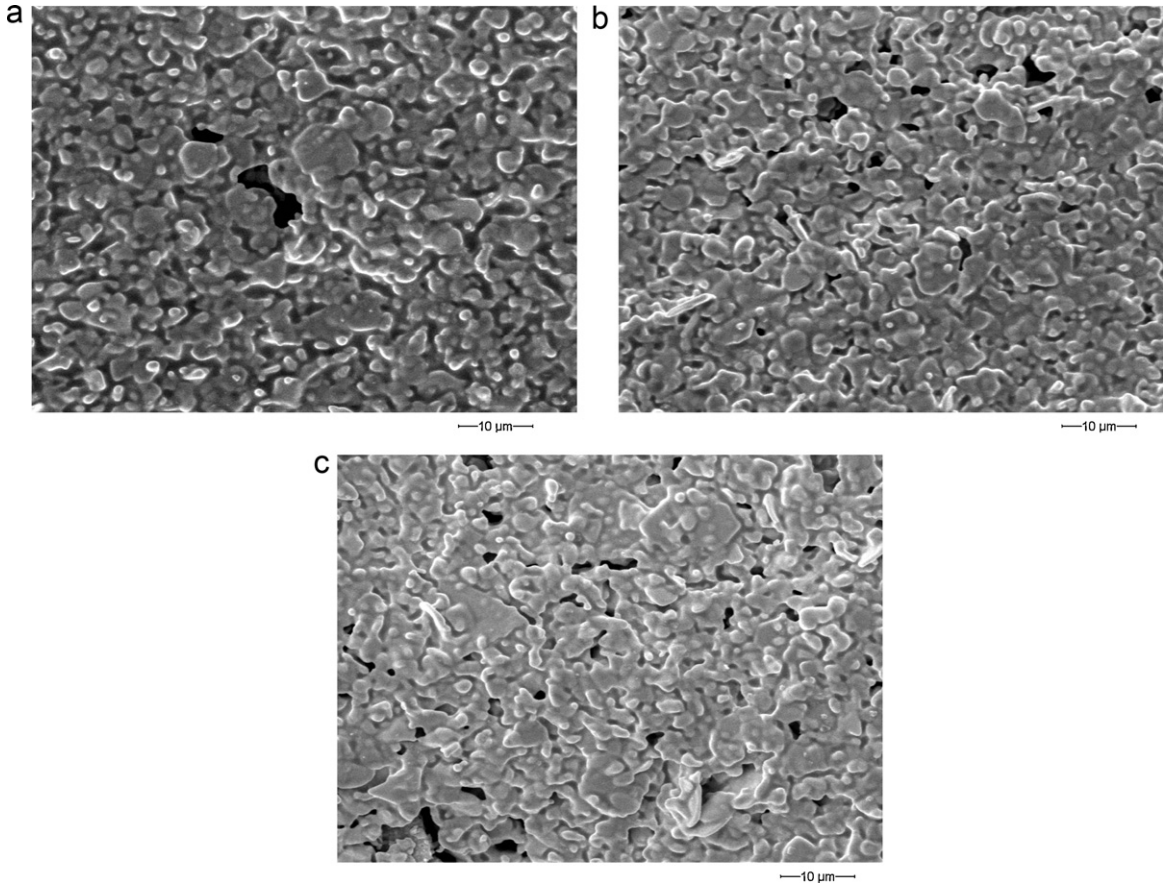

Fig. 4. SEM micrographs of 900 °C fired (a) LSF, (b) LSFC05 and (c) LSFC10.

values were determined by considering three steps, each one lasting 30 min and during which SRs' increased and settled down to a constant value. These results are comparable to the ones reported in ref. [18] on $Sm_{0.90}Sr_{0.10}CrO_3$ (ca. 180 s) and better than the other ones on $Dy_{1-x}Sr_xCrO_3$ ($0 \leq x \leq 0.1$) in Ref. [26] (about 600 s).

The sensitivity values were calculated by extrapolating the slope (m) of calibration curves obtained from the fit of experimental data, in the range in which the devices start to give a response to water vapor. In particular:

$$\frac{|R_0 - R_g|}{R_0} = m \times \mathrm{RH}\% + a \tag{2}$$

where m indicates the SR's slope, so the device's sensitivity, RH% is the value of relative humidity and a is a constant

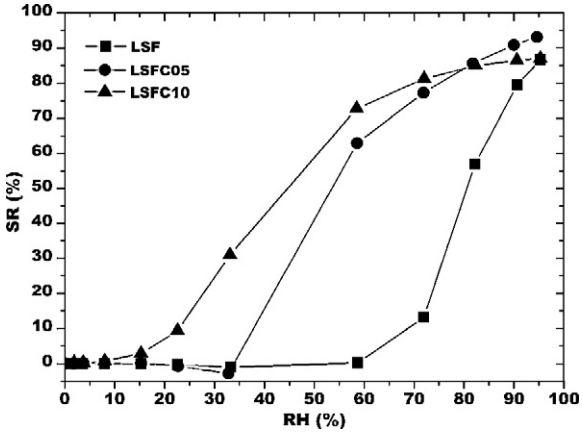

Fig. 5. SRs of LSF, LSFC05 and LSFC10 heat-treated at 800 °C in function of RH.

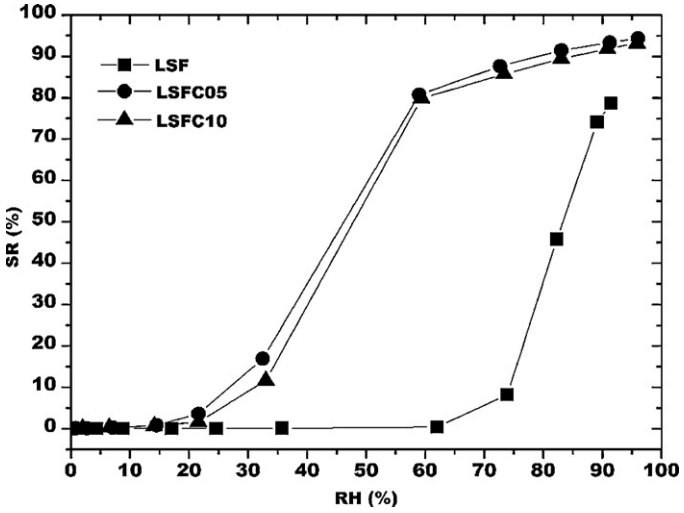

Fig. 6. SRs of LSF, LSFC05 and LSFC10 heat-treated at 900 °C in function of RH.

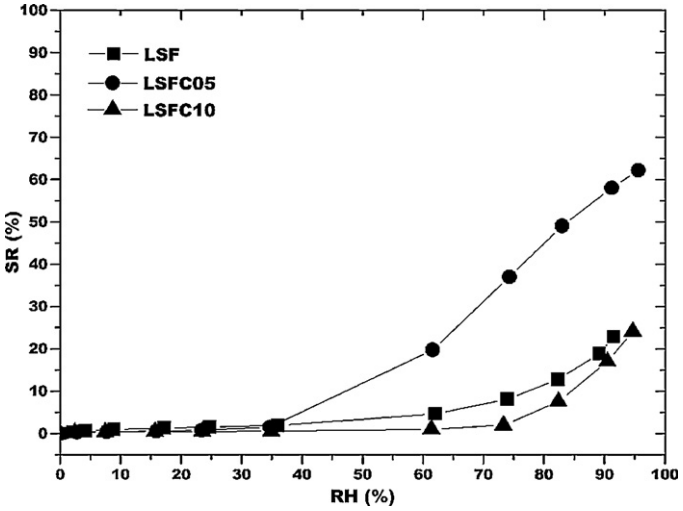

Fig. 7. SRs of LSF, LSFC05 and LSFC10 heat-treated at 1000 °C in function of RH.

number derived from the fit. The sensitivity values of the investigated sensors are reported in Table 3. By considering only the devices treated at 800 and 900 °C, the highest m belonged to LSF-based sensors ($m_{800\ °C} = 3.58 \pm 0.45$; $m_{900\ °C} = 4.09 \pm 0.23$), which showed angular coefficients much higher than those having 5% and 10% of copper; however, LSF-based sensors started to respond for higher values of RH with respect to LSFC05 and LSFC10-based sensors. Thus, the sensitivity factor tends to decrease with increasing perovskite "B" site doping.

Table 3
Sensors' sensitivity values.

Sensitivity			
Sample	m (800 °C)	m (900 °C)	m (1000 °C)
LSF	3.58 ± 0.45	4.09 ± 0.23	0.51 ± 0.09
LSFC05	2.11 ± 0.37	1.80 ± 0.24	0.97 ± 0.13
LSFC10	1.48 ± 0.17	1.82 ± 0.28	0.87 ± 0.16

The analysis of stability was carried out only for the sensors heat treated at 800 and 900 °C: the sensors were exposed alternatively to cycles under dry and humid air (at 70, 80 and 90 RH%) for three times (Figs. 8 and 9). Sensor responses were almost superposed, although considered the fluctuation caused by the manual operation of the gas microvalves.

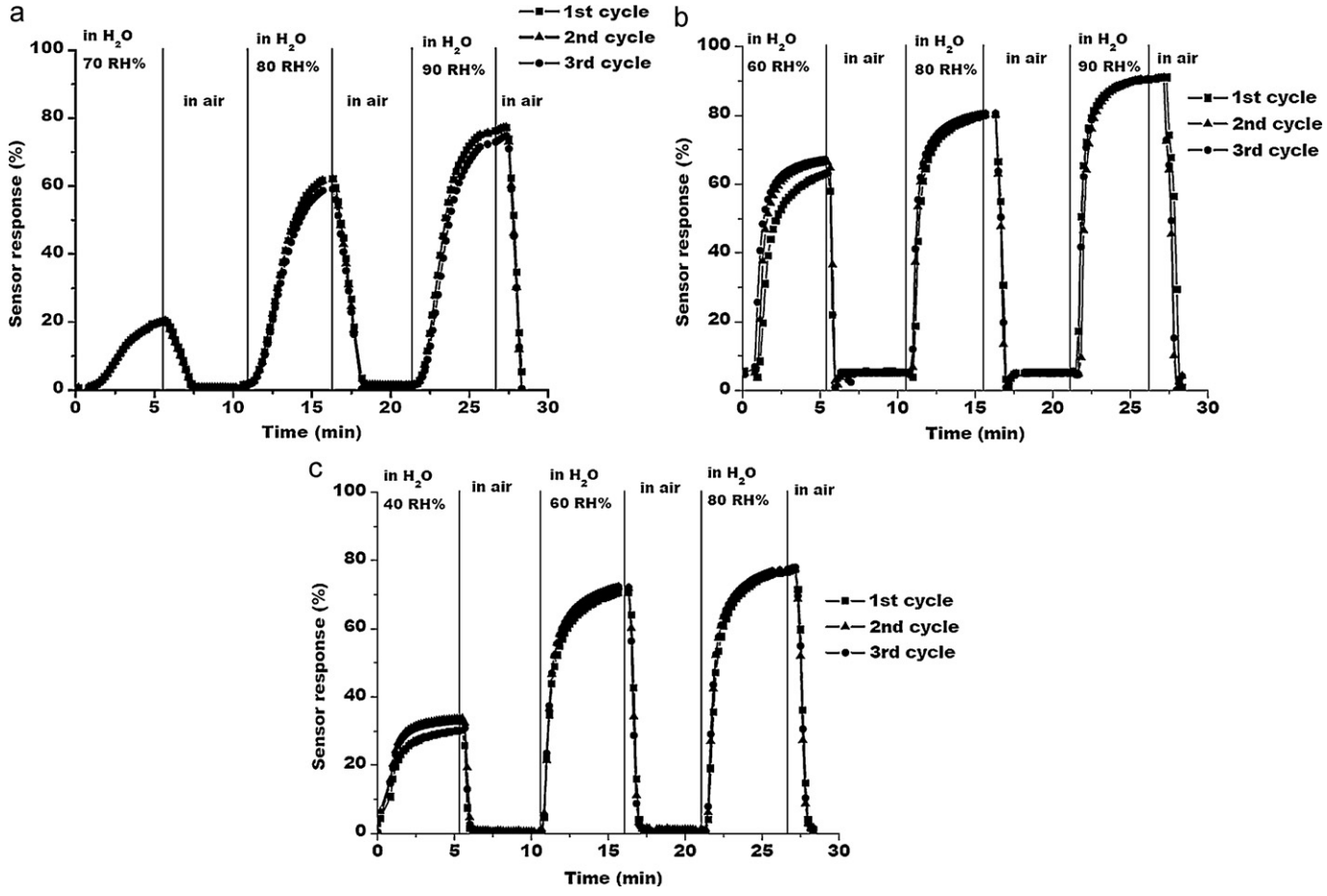

Fig. 8. Stability curves of (a) LSF, (b) LSFC05 and (c) LSFC10 treated at 800 °C.

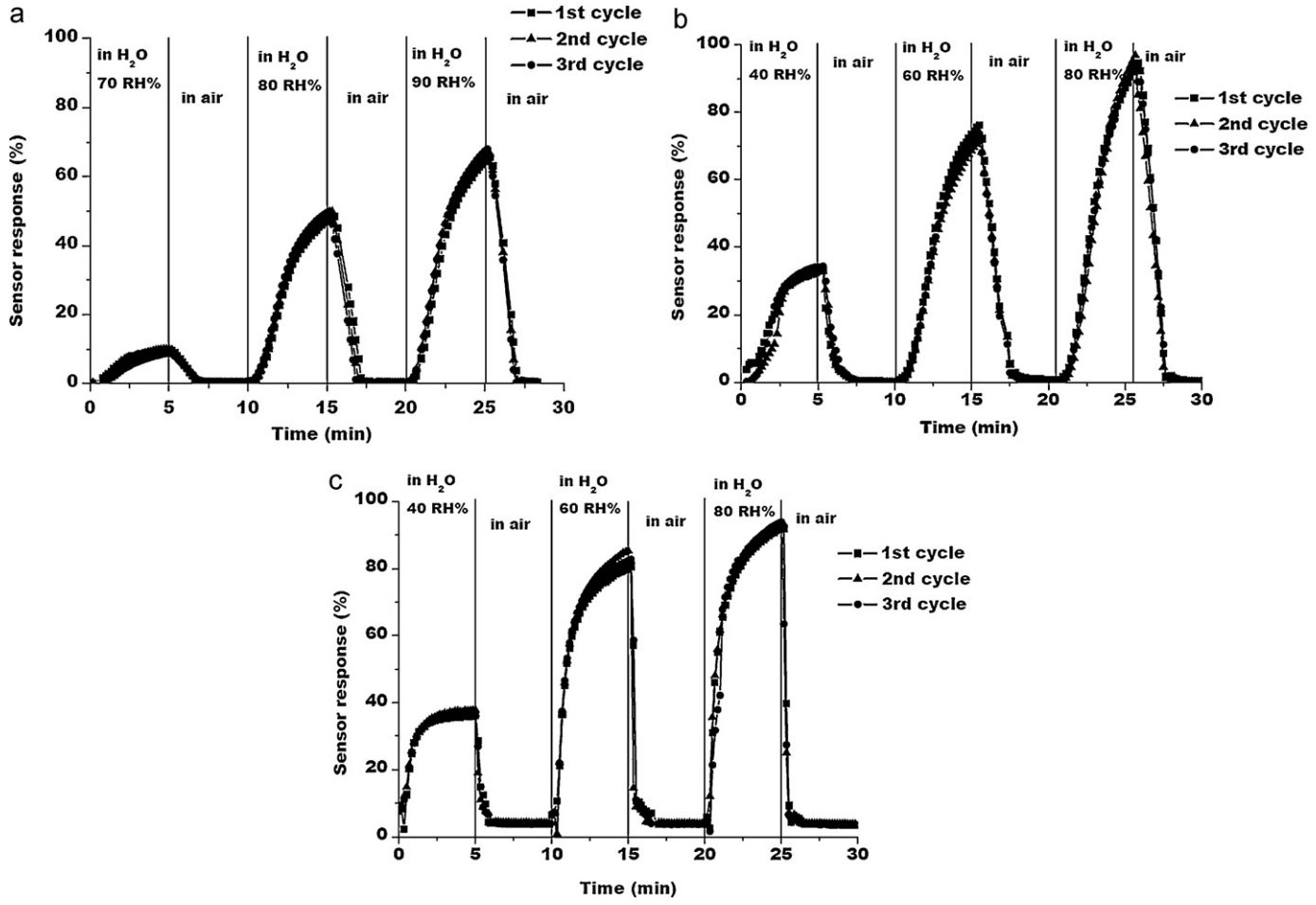

Fig. 9. Stability curves of (a) LSF, (b) LSFC05 and (c) LSFC10 treated at 900 °C.

4. Conclusions

In this work, lanthanum strontium ferrites, differing between them from the content of copper substituting iron, were proposed as sensing materials for humidity detection at room temperature. Cu-doping resulted in an increase of the specific surface area and a decrease of the crystallite size within the sensing materials.

In the absence of Cu-addition, the sensors' response were higher but, the presence of copper inside the ferrite structure brought to a variation of the sensors response to low RH values (15–30% for LSFC05 and LSFC10 compared to 65–70% for LSF).

Water condensation in the thick-films' mesoporosity proved to govern the sensors' response as these materials are known to behave as p-type semiconductors but, their resistance decreased with increasing RH values.

From these preliminary investigations, it seemed that all these materials gave very good responses under water vapor and that they could be good candidates for humidity sensors preparation.

Acknowledgment

This work was supported by the following research program: Regione Lombardia - INSTM "Catalizzatori per l'Energia e l'Ambiente Nanostrutturati (acronym CLEAN)" 2010–2012.

References

[1] J. Pérez-Ramìez, B. Vigeland, Lanthanum ferrite membranes in ammonia oxidation opportunities for "pocket-sized" nitric acid plants, Catal. Today 105 (2005) 436–442.

[2] V.A. Sadykov, L.A. Isupova, I.S. Yakovleva, G.M. Alikina, A.I. Lukashevich, S. Neophytides, Reactivity of surface and bulk oxygen in $La_{1-x}Ca_xFeO_{3-y}$ system with respect to methane oxidation, React. Kinet. Catal. Lett. 2 (2004) 393–398.

[3] D. Mescia, J.C. Caroca, N. Russo, N. Labhsetwar, D. Fino, G. Saracco, V. Specchia, Towards a single brick solution for the abatement of NO_x and soot from diesel engine exhausts, Catal. Today 137 (2008) 300–305.

[4] L.A. Isupova, G.M. Alikina, S.V. Tsybulya, A.N. Salanov, N.N. Boldyreva, E.S. Rusina, I.A. Ovsyannikova, V.A. Rogov, R.V. Bunina, V.A. Sadykov, Honeycomb-supported perovskite catalysts for high-temperature processes, Catal. Today 75 (2002) 305–315.

[5] S.P. Simner, J.F. Bonnett, N.L. Canfield, K.D. Meinhardt, J.P. Shelton, V.L. Sprenkle, J.W. Stevenson, Development of lanthanum ferrite SOFC cathodes, J. Power Sources 113 (2003) 1–10.

[6] W. Guo Wang, M. Mogensen, High-performance lanthanum-ferrite-based cathode for SOFC, Solid State Ionics 176 (2005) 457–462.

[7] S.P. Simner, J.F. Bonnett, N.L. Canfield, K.D. Meinhardt, V.L. Sprenkle, J.W. Stevenson, Optimized lanthanum ferrite-based cathodes for anode-supported SOFCs, Electrochem. Solid State Lett. 5 (2002) 173–175.

[8] H. Kishimoto, N. Sakai, T. Horita, K. Yamaji, M.E. Brito, H. Yokokawa, Cation transport behavior in SOFC cathode materials of $La_{0.8}Sr_{0.2}CoO_3$ and $La_{0.8}Sr_{0.2}FeO_3$ with perovskite structure, Solid State Ionics 178 (2007) 1317–1325.

[9] D. Burnat, P. Ried, P. Holtappels, A. Heel, T. Graule, D. Kata, The rheology of stabilised lanthanum strontium cobaltite ferrite nanopowders in organicmedium applicable as screen printed SOFC cathode layers, Fuel Cells 10 (2010) 156–165.

[10] L.T. Wilkinson, J.H. Zhu, Ag-Perovskite composite materials for SOFC cathode-interconnect contact, J. Electrochem. Soc. 156 (2009) 905–912.

[11] J.S. Yoon, J. Lee, H.J. Hwang, C.M. Whang, J. Moon, D. Kim, Lanthanum oxide-coated stainless steel for bipolar plates in solid oxide fuel cells (SOFCs), J. Power Sources 181 (2008) 281–286.

[12] J. Wang, F. Wu, G. Song, N. Wu, J. Wang, Complex impedance property of humidity sensing material lanthanum orthoferrite, Ferroelectrics 323 (2005) 71–76.

[13] S. Furfori, S. Bensaid, N. Russo, D. Fino, Towards practical application of lanthanum ferrite catalysts for NO reduction with H_2, Chem. Eng. J. 154 (2009) 348–354.

[14] N. Rezlescu, E. Rezlescu, C.-L. Sava, F. Tudorache, P.D. Popa, On the effects of Ga^{3+} and La^{3+} ions in MgCu ferrite: humidity-sensitive electrical conduction, Cryst. Res. Technol. 39 (2004) 548–557.

[15] E. Rezlescu, N. Rezlescu, F. Tudorache, P.D. Popa, Effects of replacing Fe by La or Ga in $Mg_{0.5}Cu_{0.5}Fe_2O_4$. Humidity sensitivity, J. Magn. Magn. Mater. 272–276 (2004) e1821–e1822.

[16] J. Holc, J. Slunečko, M. Hrovat, Temperature characteristics of electrical properties of (Ba,Sr)TiO_3 thick film humidity sensors, Sens. Actuators B: Chem. 26/27 (1995) 99–102.

[17] Z. Wang, L. Shi, F. Wu, S. Yuan, Y. Zhao, M. Zhang, Structure and humidity sensing properties of $La_{1-x}K_xCo_{0.3}Fe_{0.7}O_{3-\delta}$ perovskite, Sens. Actuators B: Chem. 158 (2011) 89–96.

[18] R. Sundaram, E.S. Raj, K.S. Nagaraja, Microwave assisted synthesis, characterization and humidity dependent electrical conductivity studies of perovskite oxides $Sm_{1-x}Sr_xCrO_3$ ($0 \leq x \leq 0.1$), Sens. Actuators B: Chem. 99 (2004) 350–354.

[19] Z. Jing-Li, L. Yue-Dong, W. Guo-Biao, L. Biao-Rong, Electrical conduction of $La_{1-x}Sr_x$, FeO_3, ceramics under different relative humidities, Sens. Actuators A: Phys. 29 (1991) 43–47.

[20] C.Y. Park, F.V. Azzarello, A.J. Jacobson, The oxygen non-stoichiometry and electrical conductivity of La0.7Sr0.3Cu0.2Fe0.8O3-d, J. Mater. Chem. 16 (2006) 3624–3628.

[21] M. Viviani, M.T. Buscaglia, V. Buscaglia, M. Leoni, P. Nanni, Barium perovskites as humidity sensing materials, J. Eur. Ceram. Soc. 21 (2001) 1981–1984.

[22] T. Caronna, F. Fontana, I. Natali Sora, R. Pelosato, Chemical synthesis and structural characterization of the substitution compound $LaFe_{1-x}Cu_xO_3$ ($x = 0$–0.40), Mater. Chem. Phys. 116 (2009) 645–648.

[23] H.M. Rietveld, J. Appl. Crystallogr. 2 (1969) 65, using the program GSAS written by A.C. Larson and R.B. Von Dreele, "General Structure Analysis System", Los Alamos National Laboratory Report LA-UR-86-748 (2000).

[24] J.M. Tulliani, P. Bonville, Influence of the dopants on the electrical resistance of hematite-based humidity sensors, Ceram. Int. 31 (2005) 507–514.

[25] S.E. Dann, D.B. Currie, M.T. Weller, M.F. Thomas, A.D. Al-Rawwas, The effect of oxygen stoichiometry on phase relations and structure in the system $La_{1-x}Sr_xFeO_{3-\delta}$ ($0 \leq x \leq 1$, $0 \leq \delta \leq 0.5$), J. Solid State Chem. 109 (1994) 134–144.

[26] D. Lakshmi, R. Sundaram, Humidity sensor studies on $Dy_{1-x}Sr_xCrO_3$ ($0 \leq x \leq 0.1$) synthesized by microwave assisted combustion method, Sens. Transducers J. 97 (10) (2008) 74–79.

[27] V.E. Henrich, Electron spectroscopic determination of the electronic, geometric and chemisorption properties of oxide surfaces, in: L.C. Dufour, C. Monty, G. Petot-Ervas (Eds.), Surfaces and Interfaces of Ceramic Materials, Kluwer Academic Publishers, Dordrecht, 1989, pp. 1–28.